Results in Physics 64 (2024) 107918

Contents lists available at ScienceDirect

Results in Physics

journal homepage: www.elsevier.com/locate/rinp

Bifurcation analysis and solitary wave solution of fractional longitudinal wave equation in magneto-electro-elastic (MEE) circular rod

Abdelhamid Mohammed Djaouti [a], Md. Mamunur Roshid [b], Alrazi Abdeljabbar [c,*], Ashraf Al-Quran [a]

[a] Department of Mathematics and statistic, Faculty of Science, King Faisal University, Hofuf 31982, Saudi Arabia
[b] Department of textile engineering, Uttara University (UU), Turag, Dhaka, Bangladesh
[c] Department of Mathematics, Khalifa University, Abu Dhabi, United Arab Emirates

ARTICLE INFO

Keywords:
Longitudinal Wave Equation
magneto-electro-elastic (MEE) circular rod
bifurcation Analysis
Modified simple equation method
M−fractional derivative
Magnetic material

ABSTRACT

In this study, we investigate the longitudinal wave equation (LWE) with the M−fractional derivative, which describes the propagation of longitudinal waves along a rod while incorporating interactions between mechanical, electrical, and magnetic fields within the material. Initially, we apply bifurcation analysis to examine the critical points or phase portraits where the system transitions to new behaviors, such as stability shifts or the emergence of chaos, and observe the mechanism of static soliton formation through a saddle-node bifurcation. Subsequently, we utilize a modified simple equation (MSE) technique to find solitary wave solutions. Depending on the relationships between free parameters, the solutions are expressed as hyperbolic, trigonometric, and exponential functions. The numerical form of the obtained solutions reveals complex phenomena, including dark and bright bell waves, kink periodic lump waves, kink periodic waves, periodic lump waves, interaction waves between kink and periodic waves, linked lump waves, and interactions of periodic and lump waves. Additionally, we compare our results with previously published work, demonstrating that the discussed methods are valuable tools for providing distinct, accurate soliton solutions relevant to nonlinear science and technology applications.

Introduction

In a magneto-electro-elastic (MEE) circular rod, the longitudinal wave equation is crucial for understanding the material's dynamic performance. This equation describes the propagation of longitudinal waves along the rod, accounting for interactions between mechanical, electrical, and magnetic fields. By considering material properties such as mass density and stress–strain relationships, the equation elucidates how longitudinal waves propagate through the MEE rod, exhibiting characteristics influenced by its magneto-electro-elastic nature. Additionally, the equation captures the effects of wave velocity and external forces, providing insights into the mechanisms governing wave propagation and energy transfer within the material. Understanding this model in MEE circular rods is vital for various applications, including vibration control, structural health monitoring, and the design of advanced materials for engineering and technology purposes. The proposed model in MEEC describes the transmission of longitudinal waves in cylindrical rods with elastic, electromagnetic, and magneto-electric properties. The foundational concepts of continuum mechanics and electromagnetism underpin this equation. The main goal of this effort is to investigate several invariant solitary wave solutions for the M−fractional LWE:

$$D_{M,t}^{2g,\psi}H - v^2 H_{xx} - \left(\frac{v^2}{2}H^2 + nD_{M,t}^{2g,\psi}H\right)_{xx} = 0 \tag{1}$$

Here $D_{M,t}^{2g,\psi}$ is the M−fractional operator, the term $D_{M,t}^{2g,\psi}H$ represents the acceleration of the quantity H with respect to time. In the context of wave propagation, it accounts for how the rate of change of H over time affects the overall evolution of the wave. The term $v^2 H_{xx}$ describes the curvature of the wave front along the spatial dimension x and v^2 is a constant representing the square of the wave velocity. It signifies how the wave velocity affects the spatial variation of H, influencing the propagation of the wave. The term $\left(\frac{v^2}{2}H^2 + nD_{M,t}^{2g,\psi}H\right)_{xx}$ involves a second derivative of P with respect to space (x). It captures the spatial variation of the nonlinear term $\frac{v^2}{2}H^2 + nD_{M,t}^{2g,\psi}H$. The term $\frac{v^2}{2}H^2$ represents a

* Corresponding author.
E-mail address: alrazi.abdeljabbar@ku.ac.ae (A. Abdeljabbar).

https://doi.org/10.1016/j.rinp.2024.107918
Received 16 July 2024; Received in revised form 5 August 2024; Accepted 9 August 2024
Available online 10 August 2024

nonlinear interaction within the system, while $nD_{M,t}^{2g,\psi}H$ accounts for the outcome of nonlinearity on the time fractional evolution of H. The second spatial derivative quantifies how this nonlinear interaction varies spatially, influencing the overall behavior of the system. Recently, there are many researchers investigated diverse types of solitary wave propagation of the proposed model including.

Baskonus [1] investigated the analytical exact solution of the proposed model with M fractional operator by utilizing the exp $(-\varphi(\xi))$ expansion function process, the extended trial equation process was applied to investigate new exact and explicit soliton solutions for LWE model by Seadawy [2], the novel exact and solitary wave solutions are integrated by Iqbal [3] for LWE model and they used two efficient method such as AEM and DA process, Baskonus [4] derived different wave patterns for the proposed equation by implementing the BS-E technique, Sajid [5] examined the mapping method for the proposed model to new exact and explicit solutions, W. X. Ma [6] studied the proposed model by using the modified (P'/P)-expansion method process and executed some novel traveling wave solution, Darwish [7] used the improved modified extended tanh-function method to find the exact wave solution of the proposed model in eq. (1), Ilhan [8] analyzed different wave behaviors for the proposed equation by exploiting the Sin-Gordon process, Rizvi [9] applied ansatz functions method and using a transformation in logarithmic form and they also investigated rational soliton, M shape wave and breather wave for the proposed LWE model, M. Younis [10] applied the ansatz method to construct the bright, dark, and singular solitons of the proposed model, A. Kumar [11] applied unified method and UREE technique to stimulating some wave patterns of the proposed model, A. Chakraborty [12] applied propagation in inhomogeneous one-dimensional waveguides, finite element and frequency domain SFE to analysis the longitudinal wave propagation of proposed model, H. Noufe [13] presented the exact solution and stability analysis for LWE model. the GERF method is used to generate the exact solutions, S. Gopalakrishnan [14] numerically studied the proposed model by using Super convergent finite element technique and investigated the waveguide configurations with sinusoidally varying depth, M Mamun Miah [15] investigated the singular periodic soliton and kink wave for the stochastic LWE by dual $\left(\frac{G'}{G},\frac{1}{G}\right)$-expansion method, A. Alderremy Aisha [16] studied the exact solutions and semi analytic solution for the proposed model via MAE technique and AD technique, N. Ozdemir [17] executed the bright bell, dark bell shape soliton and singular soliton solution of LWE model with M fractional operator by utilizing the UREE and NKM process, H. Bulut [18] studied the proposed equation by implementing the ES-GEE technique, K. Wang [19] examined the longitudinal wave in a 1D periodic rod with the lower band gaps by using harmonic Balance technique, A. Darwish [20] deliberated some bright soliton, singular soliton, rational soliton, singular periodic soliton of the studied model by using IMETF method, B. Ghanbari [21] investigated some peakon soliton and periodic wave soliton solutions for the LWE model by using the GERF technique in fractal media, U. Younas [22] studied singular soliton, dark soliton, bright soliton, some complex phenomena and combine of them for the proposed model by using MSS-E technique, Aly R Seadawy [23] applied Φ^6-model expansion method to the proposed equation and construct singular solution, bright-dark wave, hyperbolic, kink wave rational, trigonometric as well as Jacobi elliptic function solutions are attained, they are also checked the modulation instability of the LWE model and so on.

The principal objective of this study is to provide a detailed explanation of bifurcation analysis using phase portraits, elucidating both stable and unstable conditions, and examining homoclinic and heteroclinic solutions. Additionally, this paper integrates the M−fractional LWE model through the application of the modified simple equation (MSE) method. A.J.M. Jawad [36 applied the MSE technique to solve the Fitzhugh–Nagumo and Sharma–Tasso–Olver equations, finding exact solutions. M.M. Roshid [37,38] investigated exact and explicit solutions for the Oskolkov, KP, and modified Oskolkov equations using the MSE technique. E.M.E. Zayed [39] applied the MSE technique to study exact solutions for the nonlinear ZK-MEW and potential YTSF models. By employing the MSE method, the resulting solutions are expressed in forms such as hyperbolic, trigonometric, and rational functions, yielding 44 analytic solutions.

The structure of this work is organized as: Section 2 discusses the features and properties of the truncated M−fractional derivative, the modified simple equation technique. Section 3 focuses on the mathematical analysis of the governing model and also analyses the phase portrait, stable, unstable, homoclinic, heteroclinic, and solitary wave properties. Section 4 addresses the application of the analytical techniques. Section 5 presents the description of graphs and examines the impact of the fractional parameter. Section 6 compares the existing work with other published work, Finally, Section 7 summarizes the conclusions.

Fractional derivative

Fractional order derivatives are highly significant in scientific and engineering fields such as physics, biology, memory and hereditary properties, anomalous diffusion and transport, viscoelasticity, electrochemical systems, control theory, and signal processing. They provide a more precise and adaptable tool for modeling and understanding complex systems with anomalous behaviors, memory effects, and non-local properties that cannot be adequately captured by integer-order derivatives. Their use facilitates a more thorough explanation of complex phenomena and enhances the modeling, analysis, and control of various physical systems across multiple engineering disciplines [24,25,26,27]. Recently, various types of fractional derivatives have emerged, including the beta fractional derivative [28,29], comfy derivative [30,31], Caputo fractional derivative [32], and the recently developed M−fractional derivative [33,34,35], etc. In this work we apply the M−fractional operator to LWE model. Because of the M−fractional derivative is novel due to its ability to provide more accurate modeling by incorporating memory effects and non-local properties, distinguishing it from traditional fractional derivatives like Riemann-Liouville and Caputo, beta fractional which may not naturally accommodate initial conditions or complex system behaviors as effectively.

Definition and some features of *M*-fractional derivative.

Definition: Given a function $\varphi:[0,\infty)\rightarrow(-\infty,\infty)$ and an order, *M*-fractional derivative is well-defined as follows

$$D_{M,t}^{\chi,\psi}\varphi=\lim_{\epsilon\rightarrow0}\frac{\varphi(t\phi_{\psi}(\epsilon t^{-\chi}))-\varphi(t)}{\epsilon},t>0,\psi>0.$$

Here, $\phi_{\psi}(x)$ is a single parameter truncated Mittag-Leffler function clear as [35,36], and taking belongs to $(0,1)$:

$$\phi_{\psi}(x)=\sum_{n=0}^{k}\frac{x^{n}}{\Gamma(\phi n+1)}$$

Features. Let $0<\chi\leq1$, and $l,m\rightarrow\Re$. Let F,G be functions that are $\chi-$ differentiable at a point $t>0$. Then.

1. $D_{M,t}^{\chi,\psi}(lF+mG)=lD_{M,t}^{\chi,\psi}(F)+mD_{M,t}^{\chi,\psi}(G)$.
2. $D_{M,t}^{\chi,\psi}(FG)=FD_{M,t}^{\chi,\psi}(G)+GD_{M,t}^{\chi,\psi}(F)$.
3. $D_{M,t}^{\chi,\psi}\left(\frac{F}{G}\right)=\frac{GD_{M,t}^{\chi,\psi}(F)-FD_{M,t}^{\chi,\psi}(G)}{G^{2}}$.
4. $D_{M,t}^{\chi,\psi}(t^{\varpi})=\varpi t^{\varpi-\chi},\ \varpi\in\Re$.
5. $D_{M,t}^{\chi,\psi}(c)=0,\ c\in\Re$.
6. $D_{M,t}^{\chi,\psi}(F\circ G)=F'(G)D_{M,t}^{\chi,\psi}G(t)$, for F is differentiable at G.
7. $D_{M,t}^{\chi,\psi}F(t)=\frac{t^{1-\chi}}{\Gamma(\psi+1)}\frac{dF}{dt}$, for F is differentiable.

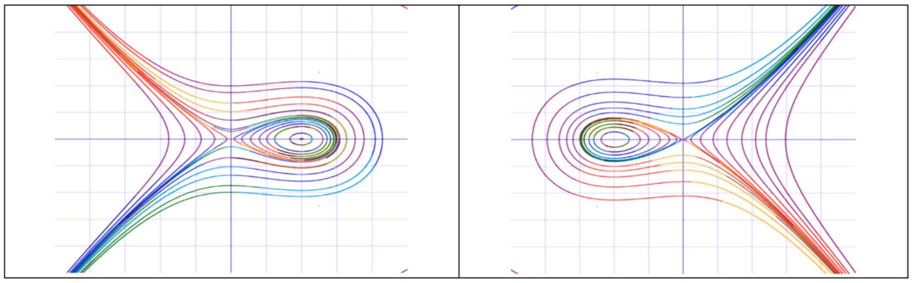

Fig. 1. Phase portrait for $2(\epsilon^2 - \nu^2\vartheta^2)\vartheta^2\epsilon^2 n > 0$.

Methodology of modified simple equation (MSE) technique

In this subsection, we elaborate on the MSE procedure [36,37,38,39] to solve NLPDEs. The MSE technique plays a significant role in integrating solitary waves of nonlinear partial differential equations (NLPDEs). Unlike methods such as the tanh–coth method [40], (G'/G) expansion technique [41], Sardar-subequation method [42], and others [42–52], the MSE technique does not rely on predefined solutions and can solve NLPDEs directly. However, its main limitations arise when the balance number exceeds two or three, making it complex to execute exact solutions. Additionally, if each term contains the derivative form of the function, the technique cannot provide any solutions. Now we consider the NLPDEs in the subsequent arrangement:

$$L(G_t, G_x, G_{xxx}, G_{tx}) = 0 \tag{2}$$

Using the relation $\zeta = \Xi x - \Theta t$; $G(x,t) = G(\zeta)$ into eq. (2) then we get:

$$L\left(-\Theta G_\zeta, \Xi G_\zeta, \Xi^3 G_{\zeta\zeta\zeta}, -\Theta\Xi G_{\zeta\zeta}\right) = 0 \tag{3}$$

The solution is:

$$G(\zeta) = \sum_{q=0}^{s}\left(p_q\left(\frac{f'(\zeta)}{f(\zeta)}\right)^q\right) \tag{4}$$

here s is the balance number happening in linear and nonlinear terms. If we insert eq. (4) into Eq. (3) then we get $P(f(\zeta)) = 0$. Setting the coefficient of each term to zero then a system of equations appears. From these equations we the values of p_q, Ξ, Θ, $f(\zeta)$, and f'. Insert these obtained values into Eq. (4), then the required solutions.

Bifurcation analysis and phase portrait

In this section, we provide a detailed explanation of bifurcation analysis using phase portraits to elucidate both stable and unstable conditions, as well as to study homoclinic and heteroclinic solutions. The time M−fractional LWE equation is considered in the following arrangement:

$$D_{M,t}^{2p,\psi}H - \nu^2 H_{xx} - \left(\frac{\nu^2}{2}H^2 + nD_{M,t}^{2g,\psi}H\right)_{xx} = 0 \tag{5}$$

Using the relation $\varphi = \vartheta x - \epsilon\frac{\Gamma(m+1)t^p}{p}$, and $H(x,t) = H(\varphi)$ into eq. (5), then we get,

$$\vartheta^2\epsilon^2 nH^{iv} + (\nu^2\vartheta^2 - \epsilon^2)H'' + \frac{\nu^2\vartheta^2}{2}(H^2)'' = 0$$

Integrating two times of the above equation and setting integrating constant to zero.

$$\vartheta^2\epsilon^2 nH'' + (\nu^2\vartheta^2 - \epsilon^2)H + \frac{\nu^2\vartheta^2}{2}H^2 = 0 \tag{6}$$

According to the Galilean transformation, Equation (6) is the following form:

$$\begin{cases} \dfrac{dH}{d\varphi} = G, \\ \dfrac{dG}{d\varphi} = \dfrac{-(\nu^2\vartheta^2 - \epsilon^2)H - \dfrac{\nu^2\vartheta^2}{2}H^2}{\vartheta^2\epsilon^2 n}, \end{cases} \tag{7}$$

$$\mathscr{H}(G,H) = \frac{G^2}{2} - \frac{1}{\vartheta^2\epsilon^2 n}\left((\epsilon^2 - \nu^2\vartheta^2)\frac{H^2}{2} - \frac{\nu^2\vartheta^2}{6}H^3\right) = L \tag{8}$$

here L is the Hamiltonian constant.

When assessing L, Eq. (8) generates a phase portrait for equation (7). Variations in L result in different types of orbits for Eq. (7), revealing diverse dynamical behaviors according to Eq. (8). To obtain the traveling wave solutions of equation (5), we will apply bifurcation analysis along with the phase diagram of equation (7). Bifurcation theory indicates that homoclinic, heteroclinic, and periodic orbits stretch growth to solitary wave, bright and dark bell, and periodic wave solutions, respectively. To integrate the equilibrium points, we set,

$$\begin{cases} G = 0, \\ \dfrac{-(\nu^2\vartheta^2 - \epsilon^2)H - \dfrac{\nu^2\vartheta^2}{2}H^2}{\vartheta^2\epsilon^2 n} = 0, \end{cases} \tag{9}$$

From the above system, the equilibrium points are $p_0 = (0,0)$ and $p_1 = \left(\frac{2(\epsilon^2-\nu^2\vartheta^2)}{\nu^2\vartheta^2}, 0\right)$. From each equilibrium point, we examine the stability. Now the linearized form of Eq. (9) has the Jacobian matrix:

$$J(p) = \begin{pmatrix} 0 & 1 \\ \dfrac{-(\nu^2\vartheta^2 - \epsilon^2) - \nu^2\vartheta^2 H_p}{\vartheta^2\epsilon^2 n} & 0 \end{pmatrix}$$

$$D(p) = -\frac{(\epsilon^2 - \nu^2\vartheta^2) - \nu^2\vartheta^2 H_p}{\vartheta^2\epsilon^2 n}$$

In the plane (G,H), the observation are:

(a) The equilibrium point represents the saddle if $D(p) < 0$.
(b) The equilibrium point is known as the center if $D(p) > 0$ and $T(p) = 0$.
(c) For $D(p) = 0$, it is referred to as the equilibrium point, and the Poincare index, or cusp point; is 0.

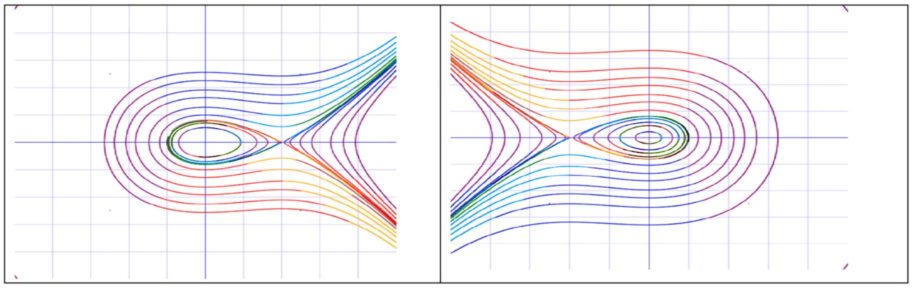

Fig. 2. Phase portraits for $2(\epsilon^2 - \nu^2\vartheta^2)\vartheta^2\epsilon^2 n < 0$.

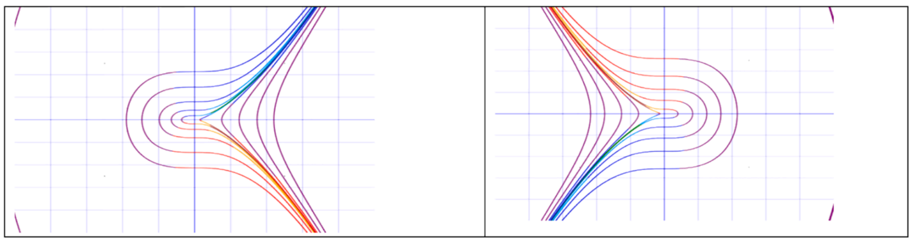

Fig. 3. Phase portraits for $\epsilon^2 = \nu^2\vartheta^2$.

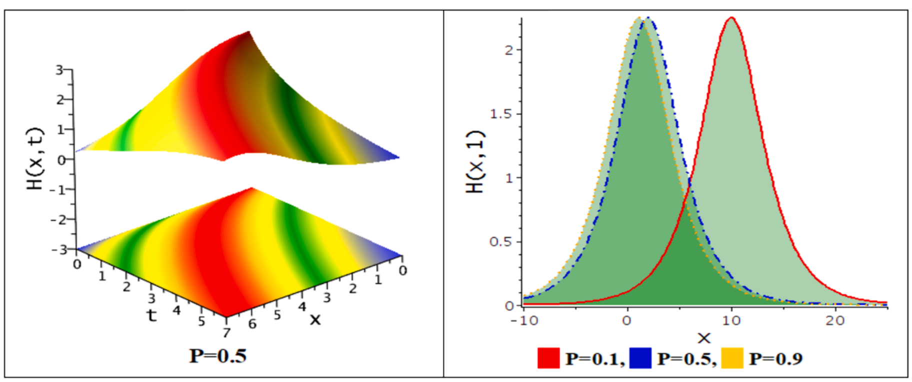

Fig. 4. 3D and 2D wave view of the solution Eq. (10) for the values $\epsilon = 1, \vartheta = 1, \nu = 2, n = 1, l = 1, g = 0.5$.

Therefore, we get,

(a) If $2(\epsilon^2 - \nu^2\vartheta^2)\vartheta^2\epsilon^2 n > 0$, then we appreciate that $D(p_1) > 0$ and $D(p_0) < 0, T(p_1) = 0$, thus the center point is p_1 and saddle point is p_0.

(b) If $2(\epsilon^2 - \nu^2\vartheta^2)\vartheta^2\epsilon^2 n < 0$, then we appreciate that $D(p_1) > 0$, $T(p_0) = 0$ and $D(p_0) < 0$, thus the center point is p_0 and saddle point is p_1.

Next, the relation of system Eq. (8) and the constant of Hamiltonian L.

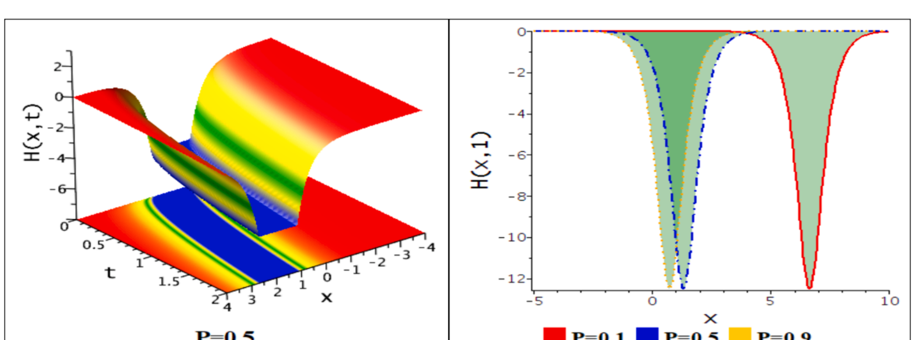

Fig. 5. 3D and 2D wave view of the Eq. (10) for the value $\epsilon = 0.5, \vartheta = 1, \nu = 0.22, n = -1, l = 1.5, g = 0.5$.

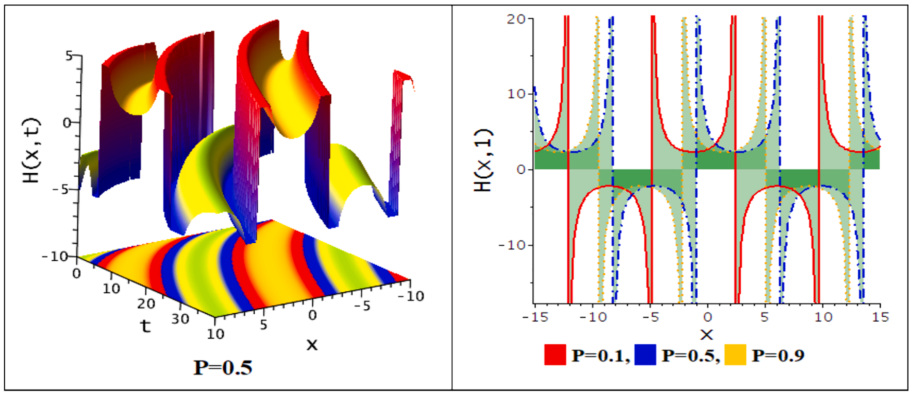

Fig. 6. 3D and 2D wave view of the Eq. (11) for the value $\epsilon = 1, \vartheta = 1, \nu = 2, n = -1, l = 1, g = 0.5$.

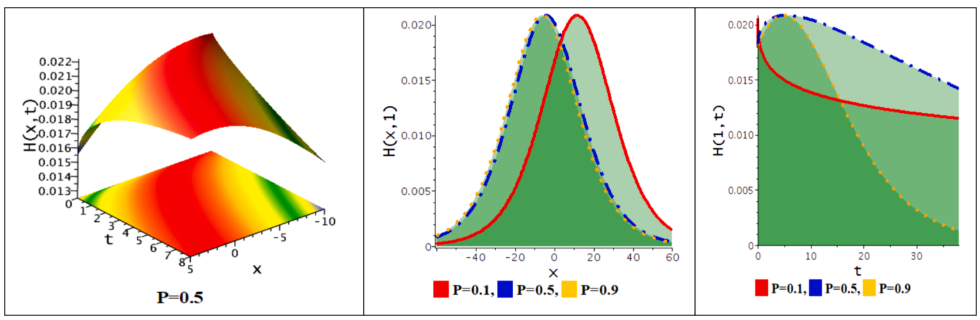

Fig. 7. Visualize the wave of the solution eq. (14) for the parametric values $\epsilon = 1, h_1 = 0.5, h_2 = 1, n = 1, \nu = 2, p_1 = 0.5$.

$$L_0 = \mathscr{H}(p_0) = 0$$

$$L_1 = \mathscr{H}(p_1) = -\frac{2(\epsilon^2 - \nu^2\vartheta^2)^3}{3\nu^4\vartheta^6\epsilon^2 n}$$

According to Figs. 1 and 2, we have the following results.

When $2(\epsilon^2 - \nu^2\vartheta^2)\vartheta^2\epsilon^2 n > 0$, we obtain

(i) For $L = L_0$, Equation (5) has a solitary wave solution corresponding to the homoclinic orbit of system (7).
(ii) For $L < L_0$, The periodic orbit of system (7) matches a periodic wave solution of equation (5).

When $2(\epsilon^2 - \nu^2\vartheta^2)\vartheta^2\epsilon^2 n < 0$, we obtain

(i) For $L = L_1$, Eq. (5) has a solitary wave solution corresponding to the homoclinic orbit of system (7).
(ii) For $L < L_1$, The periodic orbit of system (7) matches a periodic wave solution of equation (5).

By letting the Hamiltonian constant $L = 0$ here, certain diverse expressions of traveling waves of Eq. (5) are provided.

Here, some explicit expressions of traveling wave solutions of Eq. (5) are given by letting the Hamiltonian constant $L = 0$. Equation (8) can be written as

$$G = 2\sqrt{\frac{1}{\vartheta^2\epsilon^2 n}\left(\frac{(\epsilon^2 - \nu^2\vartheta^2)\mathrm{H}^2}{2} - \frac{\nu^2\vartheta^2}{6}\mathrm{H}^3\right)}$$

When $2(\epsilon^2 - \nu^2\vartheta^2)\vartheta^2\epsilon^2 n > 0$, the system (7) has a homoclinic orbit in (H, G) $-$plane. We obtain the smooth solitary wave solution

$$H(x,t) = \frac{3(\nu^2\vartheta^2 - \epsilon^2)}{\nu^2\vartheta^2} sech^2\left(\frac{1}{2}\sqrt{\frac{(\epsilon^2 - \nu^2\vartheta^2)}{\vartheta^2\epsilon^2 n}}\varphi\right) \tag{10}$$

By inserting the value of G into $dH/d\varphi = G$ and integrating then the orbit of homoclinic exist in Figs. 4 and 5 for the values $\epsilon = 1, \vartheta = 1, \nu = 2, n = 1, l = 1, g = 0.5$.

When $2(\epsilon^2 - \nu^2\vartheta^2)\vartheta^2\epsilon^2 n < 0$, then the system (5) has a heteroclinic orbit in (H, G) $-$plane. We also obtain the smooth solitary wave solution in Fig. 6 for the value $\epsilon = 1, \vartheta = 1, \nu = 2, n = -1, l = 1, g = 0.5$.

$$H(x,t) = \frac{3(\nu^2\vartheta^2 - \epsilon^2)}{\nu^2\vartheta^2} sec^2\left(\frac{1}{2}\sqrt{\frac{(\epsilon^2 - \nu^2\vartheta^2)}{\vartheta^2\epsilon^2 n}}\varphi\right) \tag{11}$$

Application of MSE technique

In this section, we apply two techniques, NMK and SE, to solve the M$-$fractional LWE model. According to the MSE technique, the trial solution is:

$$H = p_0 + p_1\frac{f'(\varphi)}{f(\varphi)} + p_2\left(\frac{f'(\varphi)}{f(\varphi)}\right)^2 \tag{12}$$

If we use Eq. (7) and its derivative form in Eq. (6), the following algebraic equations are obtained using this method.

$$\frac{1}{f(\varphi)^0} : p_0(-\nu^2\vartheta^2 + \epsilon^2) - \frac{1}{2}\nu^2\vartheta^2 p_0^2 = 0$$

$$\frac{1}{f(\varphi)} : \left(-\vartheta^2\epsilon^2 n p_1\left(\frac{d^3}{d\varphi^3}f(\varphi)\right) + p_1\left(\frac{d}{d\varphi}f(\varphi)\right)(-\nu^2\vartheta^2 + \epsilon^2) - \nu^2\vartheta^2 p_1\left(\frac{d}{d\varphi}f(\varphi)\right)p_0\right) = 0$$

$$\frac{1}{f(\varphi)^2}:\left(-g^2\epsilon^2 n\left(2p_2\left(\frac{d}{d\varphi}f(\varphi)\right)\left(\frac{d^3}{d\varphi^3}f(\varphi)\right)+2p_2\left(\frac{d^2}{d\varphi^2}f(\varphi)\right)^2-3p_1\left(\frac{d^2}{d\varphi^2}f(\varphi)\right)\left(\frac{d}{d\varphi}f(\varphi)\right)\right)+p_2\left(\frac{d}{d\varphi}f(\varphi)\right)^2(-v^2\vartheta^2+\epsilon^2)-\frac{1}{2}v^2\vartheta^2\left(2p_2\left(\frac{d}{d\varphi}f(\varphi)\right)^2p_0+p_1^2\left(\frac{d}{d\varphi}f(\varphi)\right)^2\right)\right)=0$$

$$\frac{1}{f(\varphi)^3}:-9^2\epsilon^2 n\left(-10p_2\left(\frac{d}{d\varphi}f(\varphi)\right)^2\left(\frac{d^2}{d\varphi^2}f(\varphi)\right)+2p_1\left(\frac{d}{d\varphi}f(\varphi)\right)^3\right)-v^2\vartheta^2p_2\left(\frac{d}{d\varphi}f(\varphi)\right)^3p_1=0$$

$$\frac{1}{f(\varphi)^4}:-6\vartheta^2\epsilon^2 np_2\left(\frac{d}{d\varphi}f(\varphi)\right)^4-\frac{1}{2}v^2\vartheta^2p_2^2\left(\frac{d}{d\varphi}f(\varphi)\right)^4=0$$

From first and last equations, the following solution sets are attained,

Set 01: $p_0=0, p_2=-\frac{12\epsilon^2 n}{v^2}$; **Set 02**:.$p_0=-\frac{2(v^2\vartheta^2-\epsilon^2)}{v^2\vartheta^2}, p_2=-\frac{12\epsilon^2 n}{v^2}$

Set 03:$p_0=0, \epsilon=v\sqrt{\frac{p_2}{12n}}$; **Set 04**:.$p_0=\frac{12n\vartheta^2+p_2}{6n\vartheta^2}, \epsilon=v\sqrt{\frac{p_2}{12n}}$

Set 01: Now we inset the value $p_0=0, p_2=-\frac{12\epsilon^2 n}{v^2}$ into the remaining equations and resolve them, then we get, $\vartheta=\frac{12\epsilon^2}{v}\sqrt{\frac{n}{v^2p_1^2+144n\epsilon^2}}$ and $f=h_1+h_2e^Q$.

$$H(x,t)=p_1\frac{v^2p_1\varphi}{12n\epsilon^2}\frac{h_2e^Q}{(h_1+h_2e^Q)}-\frac{12\epsilon^2 n}{v^2}\left(\frac{\frac{v^2p_1}{12n\epsilon^2}h_2e^Q}{(h_1+h_2e^Q)}\right)^2 \quad (13)$$

Here $Q=\frac{v^2p_1\varphi}{n\epsilon^2}; \varphi=\frac{12\epsilon^2}{v}\sqrt{\frac{n}{v^2p_1^2+144n\epsilon^2}}x-\epsilon\frac{\Gamma(m+1)t^p}{p}$.

If $n(v^2p_1^2+144n\epsilon^2)>0$ then the subsequent forms are derived.

If $h_1\neq h_2$, then eq.(13) becomes,

$$H(x,t)=\frac{v^2p_1^2}{12n\epsilon^2}\left[\frac{h_1h_2}{(h_1^2+h_2^2)coshQ+2h_1h_2+(h_2^2-h_1^2)sinhQ}\right] \quad (14)$$

If $h_1=h_2$, then eq.(14) becomes,

$$H(x,t)=\frac{v^2p_1^2}{12n\epsilon^2}\left[\frac{1}{2}sech\left(\frac{Q}{2}\right)\right] \quad (15)$$

If $h_1=\pm ih_2$, then eq.(14) becomes,

$$H(x,t)=\frac{v^2p_1^2}{24n\epsilon^2}\left[\frac{1}{1\mp isinhQ}\right] \quad (16)$$

If $n(v^2p_1^2+144n\epsilon^2)<0$ then the following forms are derived

If $h_1\neq h_2$, then eq.(13) becomes,

$$H(x,t)=\frac{v^2p_1^2}{12n\epsilon^2}\left[\frac{h_1h_2}{(h_1^2+h_2^2)cosQ+2h_1h_2+i(h_2^2-h_1^2)sinQ}\right] \quad (17)$$

If $h_1=h_2$, then eq. (14) becomes,

$$H(x,t)=\frac{v^2p_1^2}{12n\epsilon^2}\left[\frac{1}{2}sec\left(\frac{Q}{2}\right)\right] \quad (18)$$

If $h_1=\pm ih_2$, then eq.(14) becomes,

$$H(x,t)=\frac{v^2p_1^2}{24n\epsilon^2}\left[\frac{1}{1\pm sinQ}\right] \quad (19)$$

Here $Q=\frac{v^2p_1\varphi}{n\epsilon^2}, \varphi=\frac{12\epsilon^2}{v}\sqrt{\frac{n}{v^2p_1^2+144n\epsilon^2}}x+i\epsilon\frac{\Gamma(m+1)t^p}{p}$.

Set 02: Now we put the value of $p_0=-\frac{2(v^2\vartheta^2-\epsilon^2)}{v^2\vartheta^2}, p_2=-\frac{12\epsilon^2 n}{v^2}$ into the remaining equations and resolve them, then we get, $\vartheta=\frac{12\epsilon\sqrt{nv^2\vartheta^2-n\epsilon^2}}{\vartheta v^2}$ and $f=h_1+h_2e^Q$.

$$H(x,t)=-\frac{2(v^2\vartheta^2-\epsilon^2)}{v^2\vartheta^2}+p_1\frac{\frac{v^2p_1}{n\epsilon^2}h_2e^Q}{(h_1+h_2e^Q)}-\frac{12\epsilon^2 n}{v^2}\left(\frac{\frac{v^2p_1}{n\epsilon^2}h_2e^Q}{(h_1+h_2e^Q)}\right)^2 \quad (20)$$

Here $Q=\frac{v^2p_1\varphi}{12n\epsilon^2}; \varphi=\frac{12\epsilon\sqrt{nv^2\vartheta^2-n\epsilon^2}}{\vartheta v^2}x-\epsilon\frac{\Gamma(m+1)t^p}{p}$.

If $nv^2\vartheta^2-n\epsilon^2>0$, then the solution eq. (20) has become:

If $h_1\neq h_2$, then eq.(20) becomes,

$$H(x,t)=-\frac{2(v^2\vartheta^2-\epsilon^2)}{v^2\vartheta^2}+\frac{v^2p_1^2}{12n\epsilon^2}\left[\frac{h_1h_2}{(h_1^2+h_2^2)coshQ+2h_1h_2+(h_2^2-h_1^2)sinhQ}\right] \quad (21)$$

If $h_1=h_2$, then eq.(21) becomes,

$$H(x,t)=-\frac{2(v^2\vartheta^2-\epsilon^2)}{v^2\vartheta^2}+\frac{v^2p_1^2}{12n\epsilon^2}\left[\frac{1}{2}sech\left(\frac{Q}{2}\right)\right] \quad (22)$$

If $h_1=\pm ih_2$, then eq.(21) becomes,

$$H(x,t)=-\frac{2(v^2\vartheta^2-\epsilon^2)}{v^2\vartheta^2}+\frac{v^2p_1^2}{24n\epsilon^2}\left[\frac{1}{1\mp isinhQ}\right] \quad (23)$$

If $nv^2\vartheta^2-n\epsilon^2<0$, then the solution eq. (20) has the following form:

If $h_1\neq h_2$, then eq.(20) becomes,

$$H(x,t)=-\frac{2(v^2\vartheta^2-\epsilon^2)}{v^2\vartheta^2}+\frac{v^2p_1^2}{12n\epsilon^2}\left[\frac{h_1h_2}{(h_1^2+h_2^2)cosQ+2h_1h_2+i(h_2^2-h_1^2)sinQ}\right] \quad (24)$$

If $h_1=h_2$, then eq.(24) becomes,

$$H(x,t)=-\frac{2(v^2\vartheta^2-\epsilon^2)}{v^2\vartheta^2}+\frac{v^2p_1^2}{12n\epsilon^2}\left[\frac{1}{2}sec\left(\frac{Q}{2}\right)\right] \quad (25)$$

If $h_1=\pm ih_2$, then eq.(24) becomes,

$$H(x,t)=-\frac{2(v^2\vartheta^2-\epsilon^2)}{v^2\vartheta^2}+\frac{v^2p_1^2}{24n\epsilon^2}\left[\frac{1}{1\mp sinQ}\right] \quad (26)$$

Here $Q=i\frac{v^2p_1\varphi}{12n\epsilon^2}, \varphi=\frac{12\epsilon\sqrt{n\epsilon^2-nv^2\vartheta^2}}{\vartheta v^2}x+i\epsilon\frac{\Gamma(m+1)t^p}{p}$.

Set 03: Now we insert the value of $p_0=0, \epsilon=v\sqrt{\frac{p_2}{12n}}$ into the remaining equations and resolve them then we get two sets,

Case 01: $\vartheta=p_2\sqrt{\frac{1}{np_1^2-12np_2^2}}$ and $f=h_1+h_2e^Q$.

Now

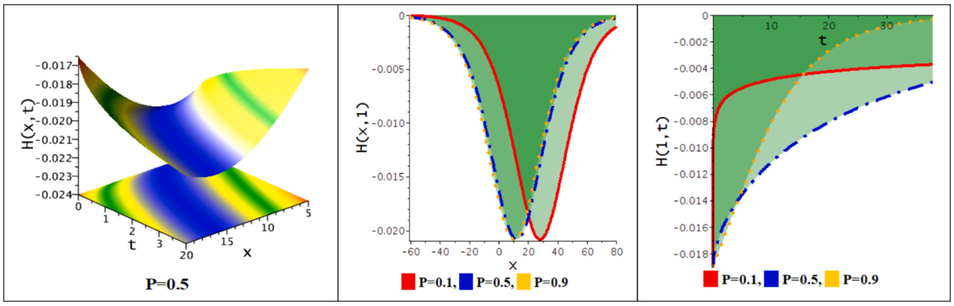

Fig. 8. Visualize the wave of the solution eq. (14) for the parametric values $\epsilon = 1, h_1 = 0.5, h_2 = 1, n = 1, \nu = 2, p_1 = 0.5$.

$$H(x,t) = p_1\frac{\frac{-p_1}{p_2}h_2e^Q}{(h_1+h_2e^Q)} + p_2\left(\frac{\frac{-p_1}{p_2}h_2e^Q}{(h_1+h_2e^Q)}\right)^2 \tag{27}$$

Here $= \frac{-p_1\varphi}{p_2}$, $\varphi = p_2\sqrt{\frac{1}{np_1^2-12np_2^2}}x - \nu\sqrt{\frac{p_2}{12n}}\frac{\Gamma(m+1)t^p}{p}$.

If $np_2 > 0$ and $np_1^2 - 12np_2^2 > 0$, then the solution eq. (27) becomes.

If $h_1 \neq h_2$, then eq. (27) becomes,

$$H(x,t) = -\frac{p_1^2}{p_2}\left[\frac{h_1h_2}{(h_1^2+h_2^2)coshQ + 2h_1h_2 + (h_2^2-h_1^2)sinhQ}\right] \tag{28}$$

If $h_1 = h_2$, then eq. (28) becomes,

$$H(x,t) = -\frac{p_1^2}{p_2}\left[\frac{1}{2}sech\left(\frac{Q}{2}\right)\right] \tag{29}$$

If $h_1 = \pm ih_2$, then eq. (28) becomes,

$$H(x,t) = -\frac{p_1^2}{p_2}\left[\frac{1}{1\mp isinhQ}\right] \tag{30}$$

If $np_2 < 0$ and $np_1^2 - 12np_2^2 < 0$, then the solution eq. (27) becomes

If $h_1 \neq h_2$, then eq. (27) becomes,

$$H(x,t) = -\frac{p_1^2}{p_2}\left[\frac{h_1h_2}{(h_1^2+h_2^2)cosQ + 2h_1h_2 + i(h_2^2-h_1^2)sinQ}\right] \tag{31}$$

If $h_1 = h_2$, then eq. (31) becomes,

$$H(x,t) = -\frac{p_1^2}{p_2}\left[\frac{1}{2}sec\left(\frac{Q}{2}\right)\right] \tag{32}$$

If $h_1 = \pm ih_2$, then eq. (31) becomes,

$$H(x,t) = -\frac{p_1^2}{p_2}\left[\frac{1}{1\mp sinQ}\right] \tag{33}$$

Here $= \frac{-p_1\varphi}{p_2}$, $\varphi = i\left(p_2\sqrt{\frac{1}{12np_2^2-np_1^2}}x - \nu\sqrt{\frac{-p_2}{12n}}t\right)$.

Case 02:$p_1 = -\sqrt{\frac{p_2^2+12n\vartheta^2p_2}{n\vartheta^2}}$; and $f = h_1 + h_2e^Q$.

Now

$$H(x,t) = -\frac{p_2^2+12n\vartheta^2p_2}{p_2n\vartheta^2}\frac{h_2e^Q}{(h_1+h_2e^Q)} + \frac{p_2^2+12n\vartheta^2p_2}{p_2n\vartheta^2}\left(\frac{h_2e^Q}{(h_1+h_2e^Q)}\right)^2 \tag{34}$$

Here $Q = \frac{\sqrt{\frac{p_2^2+12n\vartheta^2p_2}{n\vartheta^2}}\varphi}{p_2}$; $\varphi = \vartheta x - \nu\sqrt{\frac{p_2}{12n}}\frac{\Gamma(m+1)t^p}{p}$.

If $np_2 > 0$ and $n\vartheta^2(p_2^2 + 12n\vartheta^2p_2) > 0$, then the solution eq. (34) becomes.

If $h_1 \neq h_2$, then eq.(34) becomes,

$$H(x,t) = -\frac{p_2^2+12n\vartheta^2p_2}{p_2n\vartheta^2}\left[\frac{h_1h_2}{(h_1^2+h_2^2)coshQ + 2h_1h_2 + (h_2^2-h_1^2)sinhQ}\right] \tag{35}$$

If $h_1 = h_2$, then eq.(35) becomes,

$$H(x,t) = -\frac{p_2^2+12n\vartheta^2p_2}{p_2n\vartheta^2}\left[\frac{1}{2}sech\left(\frac{Q}{2}\right)\right] \tag{36}$$

If $h_1 = \pm ih_2$, then eq.(35) becomes,

$$H(x,t) = -\frac{p_2^2+12n\vartheta^2p_2}{p_2n\vartheta^2}\left[\frac{1}{1\mp isinhQ}\right] \tag{37}$$

If $np_2 < 0$ or $n\vartheta^2(p_2^2 + 12n\vartheta^2p_2) < 0$, then the solution eq. (34) becomes

If $h_1 \neq h_2$, then eq.(34) becomes,

$$H(x,t) = -\frac{p_2^2+12n\vartheta^2p_2}{p_2n\vartheta^2}\left[\frac{h_1h_2}{(h_1^2+h_2^2)cosQ + 2h_1h_2 + i(h_2^2-h_1^2)sinQ}\right] \tag{38}$$

If $h_1 = h_2$, then eq.(38) becomes,

$$H(x,t) = -\frac{p_2^2+12n\vartheta^2p_2}{p_2n\vartheta^2}\left[\frac{1}{2}sec\left(\frac{Q}{2}\right)\right] \tag{39}$$

If $h_1 = \pm ih_2$, then eq.(38) becomes,

$$H(x,t) = -\frac{p_2^2+12n\vartheta^2p_2}{p_2n\vartheta^2}\left[\frac{1}{1\mp isinQ}\right] \tag{40}$$

$$Q = i\frac{\sqrt{\frac{p_2^2+12n\vartheta^2p_2}{-n\vartheta^2}}\varphi}{p_2};\ \varphi = i\vartheta x - \nu\sqrt{\frac{-p_2}{12n}}\frac{\Gamma(m+1)t^p}{p}$$

Set 04: if we insert the value of $p_0 = \frac{12n\vartheta^2+p_2}{6n\vartheta^2}, \epsilon = \nu\sqrt{\frac{p_2}{12n}}$ into the remaining equations and resolve them, then we get two sets,

Case 01: $\vartheta = p_2\sqrt{\frac{-1}{np_1^2+12np_2}}$ and $f = h_1 + h_2e^Q$.

Now

$$H(x,t) = \frac{12n\vartheta^2+p_2}{6n\vartheta^2} + p_1\frac{\frac{-p_1}{p_2}h_2e^Q}{(h_1+h_2e^Q)} + p_2\left(\frac{\frac{-p_1}{p_2}h_2e^Q}{(h_1+h_2e^Q)}\right)^2 \tag{41}$$

Here $Q = \frac{-p_1\varphi}{p_2}, \varphi = p_2\sqrt{\frac{1}{np_1^2-12np_2^2}}x - \nu\sqrt{\frac{p_2}{12n}}\frac{\Gamma(m+1)t^p}{p}$.

If $np_1^2 - 12np_2^2 > 0$ and $np_2 > 0$, then the solutions eq. (41) becomes,

If $h_1 \neq h_2$, then eq.(41) becomes,

$$H(x,t) = \frac{12n\vartheta^2+p_2}{6n\vartheta^2} - \frac{p_1^2}{p_2}\left[\frac{h_1h_2}{(h_1^2+h_2^2)coshQ + 2h_1h_2 + (h_2^2-h_1^2)sinhQ}\right] \tag{42}$$

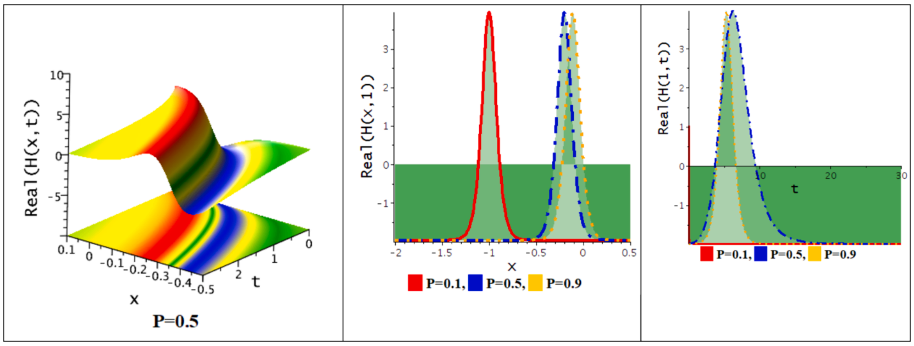

Fig. 9. Visualize the wave of the solution eq. (23) for the parametric values $\epsilon = -0,2, n = 1, \nu = -1, \vartheta = 2$.

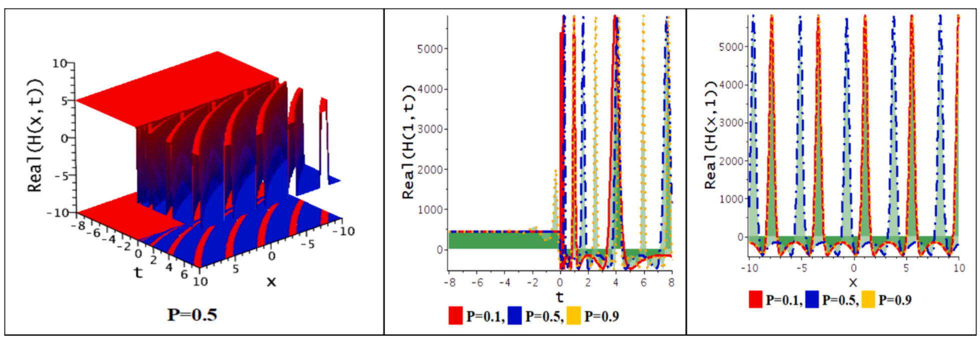

Fig. 10. Visualize the wave of the solution eq. (24) for the parametric values $\epsilon = 1, h_1 = 0.5, h_2 = 1, n = 0.5, \nu = 0.2, \vartheta = 0.33$.

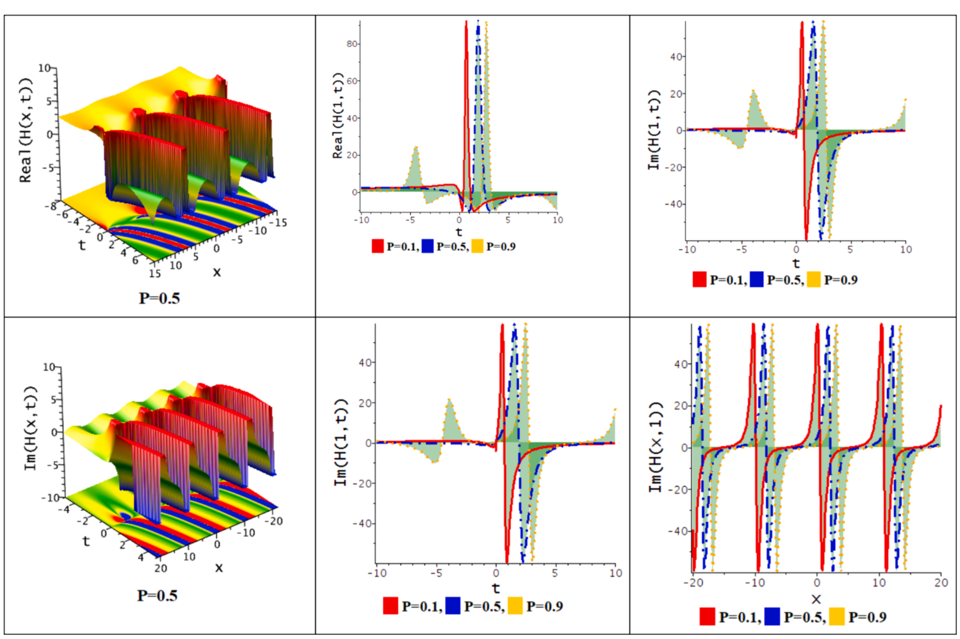

Fig. 11. Visualize the wave of the solution eq. (24) for the parametric values $\epsilon = 1.5, h_1 = 1, h_2 = 1.5, n = 1.5, \nu = -1, \vartheta = -1$.

If $h_1 = h_2$, then eq.(42) becomes,

$$H(x,t) = \frac{12n\vartheta^2 + p_2}{6n\vartheta^2} - \frac{p_1^2}{p_2}\left[\frac{1}{2}sech\left(\frac{Q}{2}\right)\right] \tag{43}$$

If $h_1 = \pm ih_2$, then eq.(42) becomes,

$$H(x,t) = \frac{12n\vartheta^2 + p_2}{6n\vartheta^2} - \frac{p_1^2}{p_2}\left[\frac{1}{1 \mp isinhQ}\right] \tag{44}$$

If $np_1^2 - 12np_2^2 < 0$ and $np_2 < 0$, then the solutions eq. (41) becomes,
If $h_1 \neq h_2$, then eq.(41) becomes,

$$H(x,t) = \frac{12n\vartheta^2 + p_2}{6n\vartheta^2} - \frac{p_1^2}{p_2}\left[\frac{h_1h_2}{(h_1^2 + h_2^2)cosQ + 2h_1h_2 + i(h_2^2 - h_1^2)sinQ}\right] \tag{45}$$

If $h_1 = h_2$, then eq.(45) becomes,

$$H(x,t) = \frac{12n\vartheta^2 + p_2}{6n\vartheta^2} - \frac{p_1^2}{p_2}\left[\frac{1}{2}sec\left(\frac{Q}{2}\right)\right] \tag{46}$$

If $h_1 = \pm ih_2$, then eq.(45) becomes,

$$H(x,t) = \frac{12n\vartheta^2 + p_2}{6n\vartheta^2} - \frac{p_1^2}{p_2}\left[\frac{1}{1 \mp sinQ}\right] \tag{47}$$

Here $= \frac{-p_1\varphi}{p_2}$, $\varphi = i\left(p_2\sqrt{\frac{-1}{np_1^2 - 12np_2^2}}x - \nu\sqrt{\frac{-p_2}{12n}}\ \frac{\Gamma(m+1)t^p}{p}\right)$.

Case 02:.$p_1 = \frac{1}{\vartheta}\sqrt{\frac{12n\vartheta^2p_2 + p_2^2}{-n}}$

Now

$$H(x,t) = \frac{12n\vartheta^2 + p_2}{6n\vartheta^2} + \frac{-\frac{p_1^2}{p_2}h_2e^Q}{(h_1 + h_2e^Q)} - \frac{12n\vartheta + \sqrt{144n^2\vartheta^2 - 4np_1^2}}{2}\left(\frac{\frac{-p_1}{p_2}h_2e^Q}{(h_1 + h_2e^Q)}\right)^2 \tag{48}$$

Here $Q = \frac{p_1\varphi}{\frac{12n\vartheta + \sqrt{144n^2\vartheta^2 - 4np_1^2}}{2}}$; $\varphi = \vartheta x - \nu\sqrt{\frac{p_2}{12n}}\ \frac{\Gamma(m+1)t^p}{p}$.

If $p_2n > 0$ then the solutions eq. (48) becomes,
If $h_1 \neq h_2$, then eq.(48) becomes,

$$H(x,t) = \frac{12n\vartheta^2 + p_2}{6n\vartheta^2} + \frac{p_1^2}{\frac{12n\vartheta + \sqrt{144n^2\vartheta^2 - 4np_1^2}}{2}}\left[\frac{h_1h_2}{(h_1^2 + h_2^2)coshQ + 2h_1h_2 + (h_2^2 - h_1^2)sinhQ}\right] \tag{49}$$

If $h_1 = h_2$, then eq.(49) becomes,

$$H(x,t) = \frac{12n\vartheta^2 + p_2}{6n\vartheta^2} + \frac{p_1^2}{\frac{12n\vartheta + \sqrt{144n^2\vartheta^2 - 4np_1^2}}{2}}\left[\frac{1}{2}sech\left(\frac{Q}{2}\right)\right] \tag{50}$$

If $h_1 = \pm ih_2$, then eq. (49) becomes,

$$H(x,t) = \frac{12n\vartheta^2 + p_2}{6n\vartheta^2} + \frac{p_1^2}{\frac{12n\vartheta + \sqrt{144n^2\vartheta^2 - 4np_1^2}}{2}}\left[\frac{1}{1 \mp isinhQ}\right] \tag{51}$$

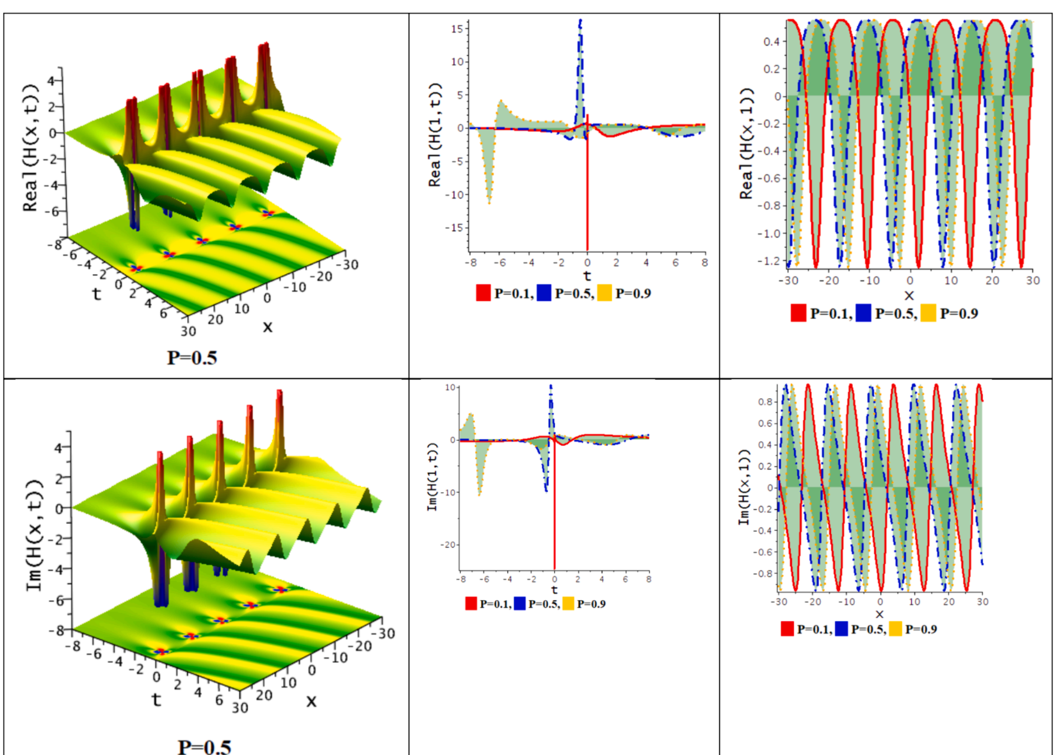

Fig. 12. Visualize the wave of the solution eq. (31) for the parametric values $p_1 = 1, p_2 = -0.25, h_1 = 1, h_2 = -0.5, n = -1, \nu = 2, \vartheta = 0.33$.

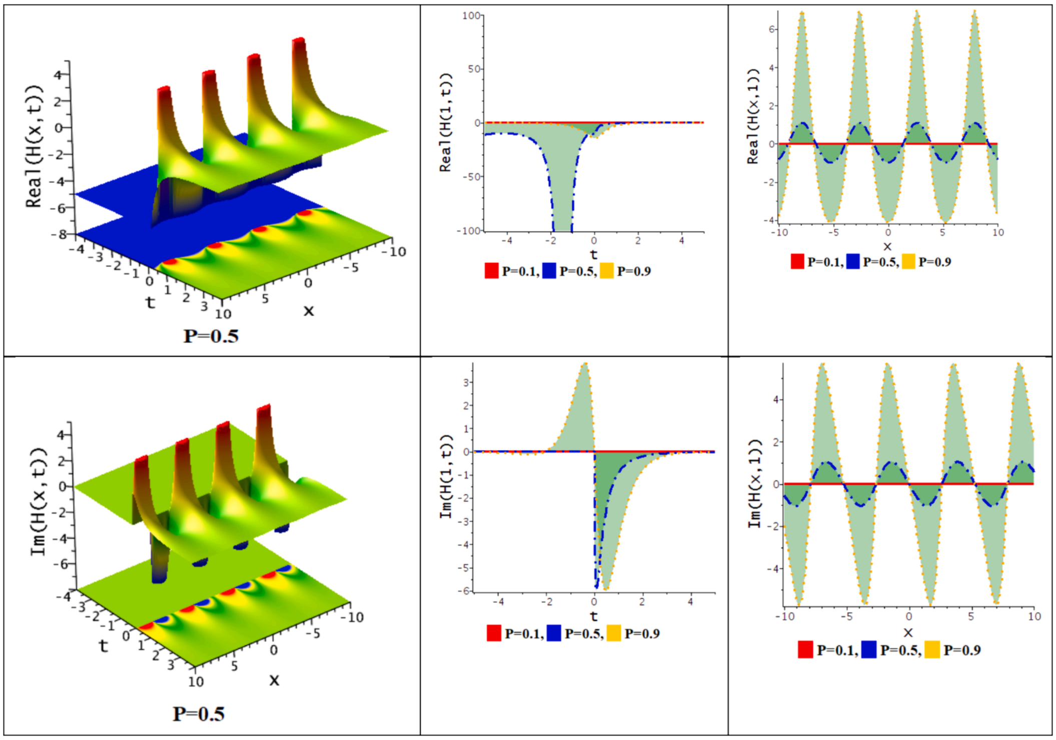

Fig. 13. Visualize the wave of the solution eq. (33) for the parametric values $p_1 = 2, p_2 = 0.1, n = -1, \nu = 1, \vartheta = 0.33$.

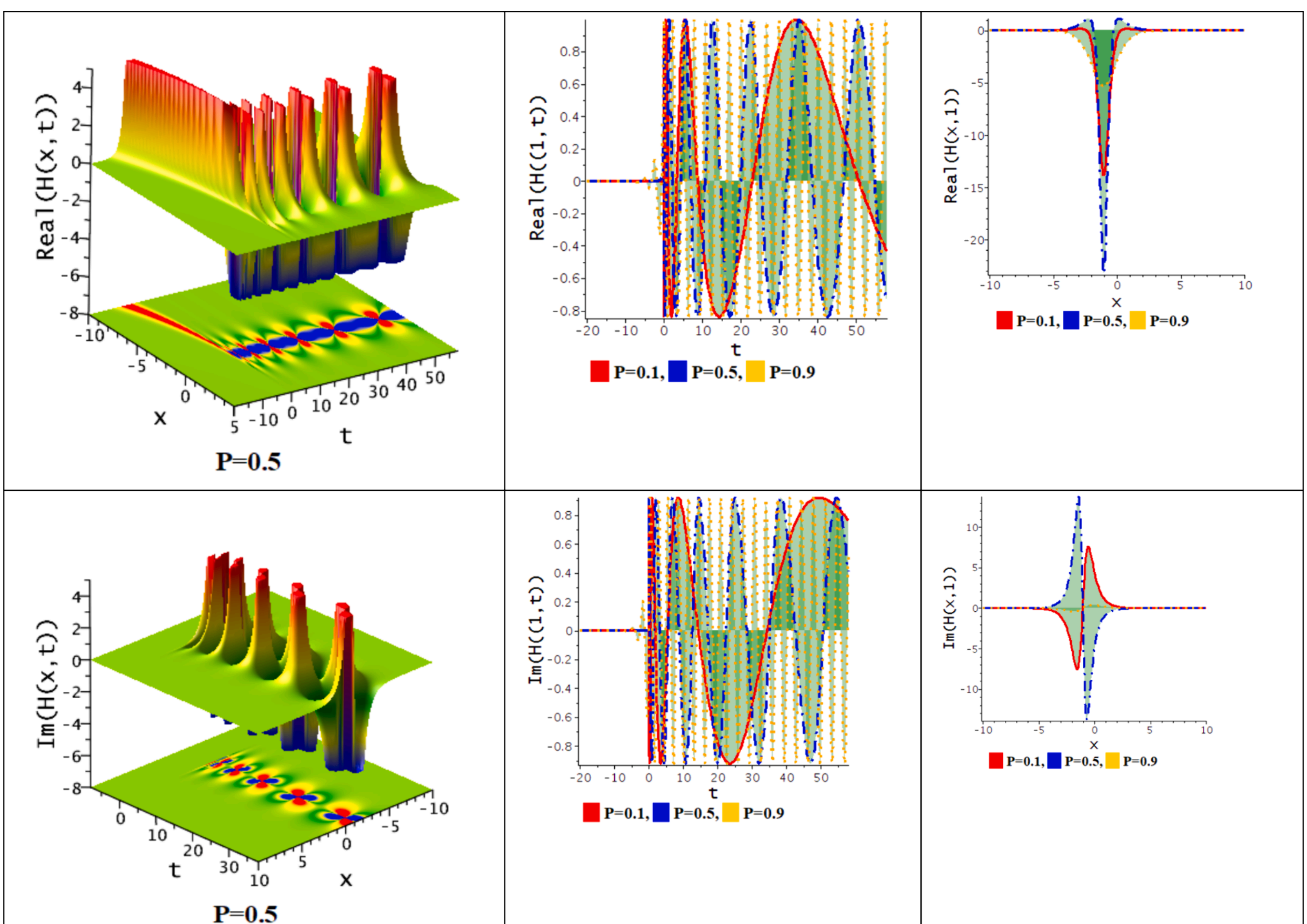

Fig. 14. Visualize the wave of the solution eq. (38) for the parametric values $\vartheta = 1, p_2 = 1, h_1 = 1, h_2 = -0.5, n = 1, \nu = 2, \vartheta = 0.33$.

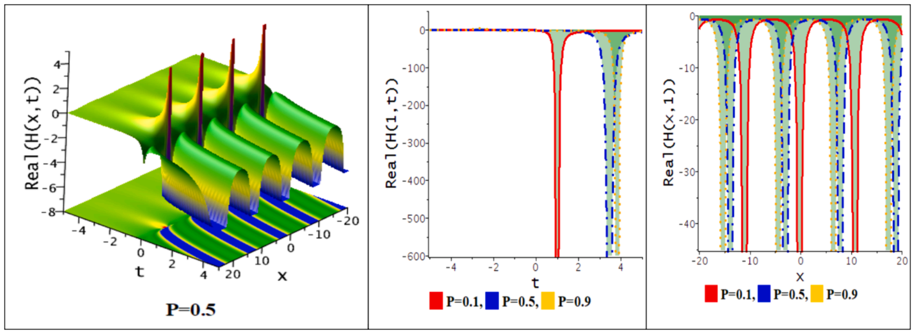

Fig. 15. Visualize the wave of the solution eq. (39) for the parametric values $\vartheta = 1, p_2 = -1, n = 1, \nu = 2$.

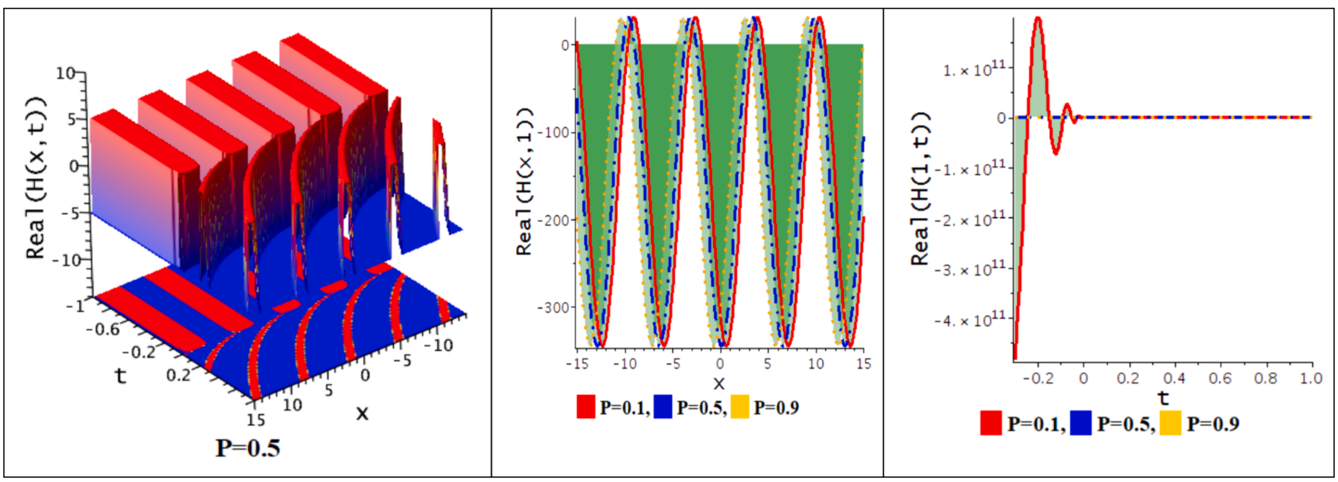

Fig. 16. Visualize the wave of the solution eq. (45) for the parametric values $\vartheta = 0.1, p_2 = -2, n = 1, \nu = 2, p_1 = 0.5$.

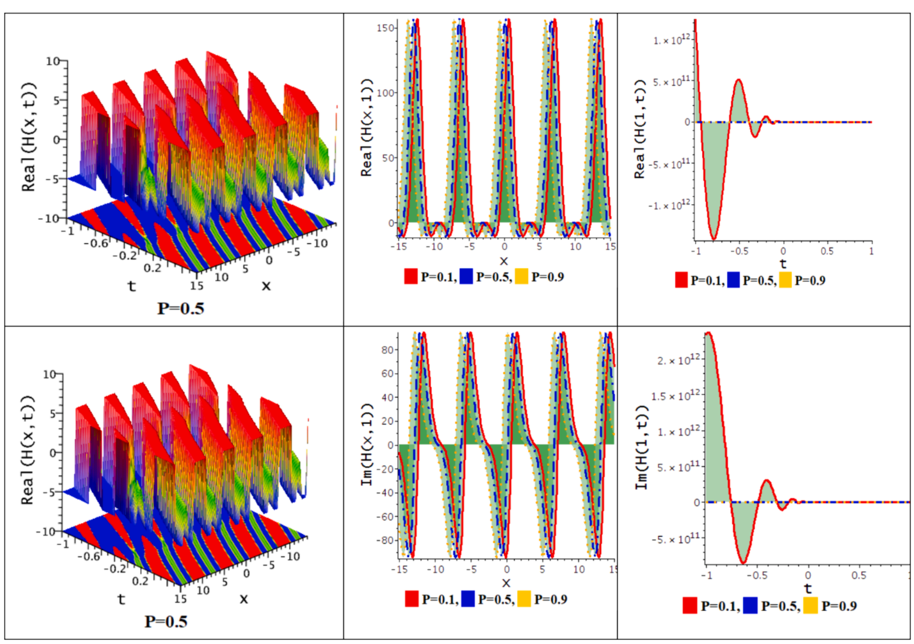

Fig. 17. Visualize the wave of the solution eq. (45) for the parametric values $\vartheta = 0.1, h_1 = 1, h_2 = 0.33, p_2 = -2, n = 1, \nu = 2, p_1 = 0.5$.

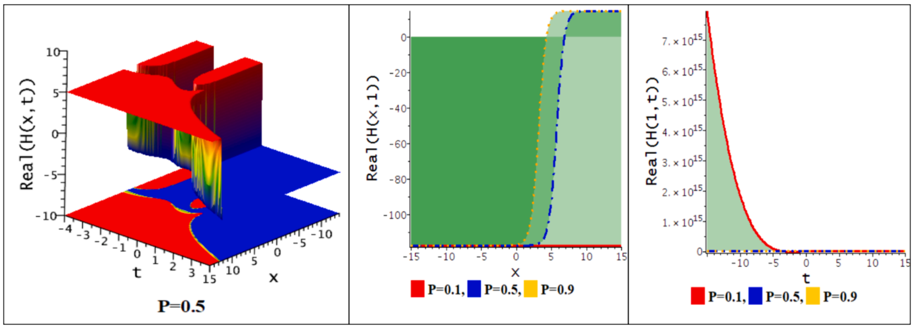

Fig. 18. Visualize the wave of the solution eq. (47) for the parametric values $\vartheta = 0.1, p_2 = 1, n = -1, \nu = 1, p_1 = 0.5$.

If $p_2 n < 0$ then the solutions eq. (48) becomes,

If $h_1 \neq h_2$, then eq.(48) becomes,

$$H(x,t) = \frac{12n\vartheta^2 + p_2}{6n\vartheta^2} + \frac{p_1^2}{\frac{12n\vartheta + \sqrt{144n^2\vartheta^2 - 4np_1^2}}{2}}\left[\frac{h_1h_2}{(h_1^2 + h_2^2)cosQ + 2h_1h_2 + i(h_2^2 - h_1^2)sinQ}\right] \tag{52}$$

If $h_1 = h_2$, then eq.(52) becomes,

$$H(x,t) = \frac{12n\vartheta^2 + p_2}{6n\vartheta^2} + \frac{p_1^2}{\frac{12n\vartheta + \sqrt{144n^2\vartheta^2 - 4np_1^2}}{2}}\left[\frac{1}{2}sec\left(\frac{Q}{2}\right)\right] \tag{53}$$

If $h_1 = \pm ih_2$, then eq. (52) becomes,

$$H(x,t) = \frac{12n\vartheta^2 + p_2}{6n\vartheta^2} + \frac{p_1^2}{\frac{12n\vartheta + \sqrt{144n^2\vartheta^2 - 4np_1^2}}{2}}\left[\frac{1}{1 \mp isinQ}\right] \tag{54}$$

Here $Q = \frac{p_1\varphi}{\frac{12n\vartheta + \sqrt{144n^2\vartheta^2 - 4np_1^2}}{2}}; \varphi = i\left(-i\vartheta x - \nu\sqrt{\frac{-p_2}{12n}}\frac{\Gamma(m+1)t^p}{p}\right)$.

Result and discussion

In this division, we examine the graphical depictions of the solutions we have found. These solutions are graphically represented by the waveforms shown below. Using in-depth justifications and supporting graphics, we thoroughly examine the behavior and distinctive features of the solutions generated from the M−fractional LWE equations. The solitary wave solutions are most important in a magneto-electro-elastic (MEE) circular rod lies of their ability to provide insights into the complex interactions between magnetic, electric, and mechanical fields. The numerical form of the obtained solutions is illustrated with 3D and 2D plots such as bright and dark bell shape waves, kink periodic lump waves, kink periodic waves, periodic lump waves, interaction waves between kink and periodic waves, linked lump waves, the interaction of periodic wave and lump wave, the periodic wave, kink, and periodic wave. These solutions help characterize material properties, inform the design of advanced sensors and actuators, and enable efficient energy transfer and signal processing. Studying solitary waves in MEE materials also enhances the understanding of nonlinear wave dynamics and stability, driving the development of innovative applications and improving the accuracy of theoretical models in the field of smart materials and structures. These solutions are crucial for designing advanced MEE materials and devices, enhancing performance in applications like vibration control, structural health monitoring, and energy harvesting. By understanding these wave dynamics, researchers can optimize MEE systems for improved efficiency and functionality. Their roles in manipulating wave propagation and energy transfer within the material. The bright type solitary waves form, when the energy from mechanical, electrical, and magnetic fields constructively interferes, leading to increased amplitude. Dark type solitary waves result from destructive interference, causing reduced amplitude. Periodic waves arise from the continuous and repetitive interaction of these fields, creating consistent wave patterns. These mechanisms help in precisely controlling wave propagation and energy distribution within MEE materials, crucial for applications in vibration control, structural health monitoring, and energy harvesting. In Figs. 7 to 18, we illustrated some phenomena of M-fractional LWE equations such as. The effect of comfortable fractional parameters is shown in two-dimensional plots at $g = 0.1, 0.5, 0.9$. We also have the three-dimensional plot for $g = 0.5$. Fig. 7, visualizes the bright bell wave of the solution eq. (14) for the parametric values $\in = 1$, $h_1 = 0.5, h_2 = 1, n = 1, \nu = 2, p_1 = 0.5$. Fig. 8 Visualizes the 3D and 2D diagram of the dark bell shape wave of the solution eq. (14) for the parametric values $\in = 1, h_1 = 0.5, h_2 = 1, n = 1, \nu = 2, p_1 = 0.5$. Fig. 9 Visualizes the 3D and 2D plots of bright and dark bell shape waves of the solution eq. (23) for the parametric values $\in = -0{,}2, n = 1, \nu = -1, \vartheta = 2$. The solution eq. (24) represented the kink periodic wave and the 3D and 2D plots illustrate these phenomena in Fig. 10 for the parametric values $\in = 1, h_1 = 0.5, h_2 = 1, n = 0.5, \nu = 0.2, \vartheta = 0.33$. Fig. 11 Visualizes the 3D and 2D plots of kinky periodic lump wave of the solution eq. (24) for the parametric values $\in = 1.5, h_1 = 1, h_2 = 1.5, n = 1.5, \nu = -1, \vartheta = -1$. The solution eq. (31) represents the periodic lump wave and the 3D and 2D plots are illustrated of this phenomena in Fig. 12 for the parametric values $p_1 = 1, p_2 = -0.25, h_1 = 1, h_2 = -0.5, n = -1, \nu = 2, \vartheta = 0.33$.Fig. 13 Visualizes the 3D and 2D plots of the interaction wave between the kink and periodic wave of the solution eq. (33) for the parametric values $p_1 = 2, p_2 = 0.1, n = -1, \nu = 1, \vartheta = 0.33$. Fig. 14 Visualizes the linked lump wave of the solution eq. (38) for the parametric values $\vartheta = 1, p_2 = 1, h_1 = 1, h_2 = -0.5, n = 1, \nu = 2, \vartheta = 0.33$. Fig. 15 visualizes the interaction of the periodic wave and lump wave of the solution eq. (39) for the parametric values $\vartheta = 1, p_2 = -1, n = 1, \nu = 2$. The solution eq. (45) represents the periodic wave and the 3D and 2D plots illustrate these phenomena in Fig. 16 for the parametric values $p_1 = 1, p_2 = -0.25, h_1 = 1, h_2 = -0.5, n = -1, \nu = 2, \vartheta = 0.33$. Fig. 17 Visualizes the periodic wave of the solution eq. (45) for the parametric values $\vartheta = 0.1, h_1 = 1, h_2 = 0.33, p_2 = -2, n = 1, \nu = 2, p_1 = 0.5$. The solution eq. (47) represents the interaction of kink and periodic wave and the 3D and 2D plots are illustrated of this phenomena in Fig. 18 for the parametric values $p_1 = 1, p_2 = -0.25, h_1 = 1, h_2 = -0.5, n = -1$,

$\nu = 2, \vartheta = 0.33$.

Comparison and novelty

It is important to note that the techniques we employed are straightforward and require less computational effort compared to other methods [23,27]. These techniques do not rely on auxiliary equations or predefined solutions, allowing for a clearer understanding of the model's internal mechanisms. Aljahdaly [23] addressed the same model using the new generalized exponential rational function method and obtained solutions such as bright bell, dark bell, kink-shaped, and periodic solitary wave solutions. Similarly, Ozdemir [27] applied the unified Riccati equation expansion and the new Kudryashov methods to solve the LWE, deriving soliton solutions like periodic and singular solutions in real form with the aid of auxiliary equations. Our methods, however, produced solitary, periodic, and singular solutions in both real and complex forms, encompassing all previously reported solutions. Additionally, we derived our results through direct integration from the Hamiltonian, following each energy orbit of its phase portraits. This led to the discovery of various bright and dark bell-shaped waves, kinky periodic lump waves, kink periodic waves, periodic lump waves, interaction waves between kink and periodic waves, linked lump waves, interactions of periodic waves and lump waves, and periodic waves, including kink and periodic wave solutions of the LWE model, which were not reported in [11–34].

Conclusion

In this framework, we have successfully studied the M−fractional longitudinal waves equation by using bifurcation analysis, and MSE technique. By implementing bifurcation analysis, we can explain the stability of the proposed model. In Figs. 1–3, we show some diagrams of the phase portrait of the LWE model and also derive some homoclinic and solitary wave solutions. This study, used the MSE technique for the propagation of longitudinal waves along the length of the rod, accounting for interactions between mechanical, electrical, and magnetic fields within the material. Under some conditions, we obtained the analytic form of the obtained solutions in terms of trigonometric, hyperbolic, and exponential form. To explain the wave's propagation, we discussed the obtained solutions numerically and graphically. Through the assistance of the suggested approach, the solitary wave propagation of M−fractional LWE was successfully found, illuminating complex and various structures including bright and dark bell-shaped waves, kinky periodic lump waves, kink periodic waves, periodic lump waves, interaction waves between kink and periodic waves, linked lump waves, interactions of periodic waves and lump waves, and periodic waves, including kink and periodic wave solutions. It is important to recognize that these findings shed light on one of the most fascinating problems in magneto-electro-elastic (MEE) circular rod technology. This research has improved mathematical physics in addition to the material's mechanical, electrical, and magnetic fields. The study's findings are encouraging for fundamental scientific knowledge as well as for potential beneficial applications in the areas of mechanical, electrical, and magnetic fields within the material. Future work in acquiring the various types of soliton solutions for the NLPDEs will benefit from this study. The proposed approach is a powerful way to find the exact solutions for the integral differential equations.

CRediT authorship contribution statement

Abdelhamid Mohammed Djaouti: Validation, Methodology, Conceptualization. **Md. Mamunur Roshid:** Writing – original draft, Methodology, Formal analysis. **Alrazi Abdeljabbar:** Writing – review & editing, Validation, Supervision, Methodology, Investigation. **Ashraf Al-Quran:** Validation, Methodology, Investigation, Formal analysis.

Declaration of competing interest

The authors declare that they have no known competing financial interests or personal relationships that could have appeared to influence the work reported in this paper.

Data availability

No data was used for the research described in the article.

Acknowledgement

This work was supported by the Deanship of Scientific Research, Vice Presidency for Graduate Studies and Scientific Research, King Faisal University, Saudi Arabia (Project No. KFU241538). Additionally, this research received funding from Khalifa University, Abu Dhabi, United Arab Emirates.

References

[1] Baskonus HM, Bulut H, Atangana A. On the complex and hyperbolic structures of the longitudinal wave equation in a magneto-electro-elastic circular rod. Smart Mater Struct 2016;25:035022.
[2] Seadawy AR, Manafian J. New soliton solution to the longitudinal wave equation in a magneto-electro-elastic circular rod. Result Phys 2018;8:1158–67.
[3] Iqbal M, Seadawy AR, Lu D. Applications of nonlinear longitudinal wave equation in a magneto-electro-elastic circular rod and new solitary wave solutions. Mod Phys Lett b 2019;3:1950210.
[4] Baskonus HM, Gomez-Aguilar JF. New singular soliton solutions to the longitudinal wave equation in a magneto-electro-elastic circular rod with M -derivative. Mod Phys Lett b 2019;33:1950251.
[5] Sajid N, Akram G. Solitary dynamics of longitudinal wave equation arises in magneto-electroelastic circular rod. Mod Phys Lett b 2021;35:2150086.
[6] Ma X, Pan Y, Chang L. Explicit travelling wave solutions in a magneto-electro-elastic circular rod. Int J Comput Sci Issues 2013;10(1):62–8.
[7] Darwish A, Seadawy AR, Ahmed HM, Elbably AL, Shehab MF, Arnous AH. Study on soliton solutions of the longitudinal wave equation and magneto-electro-elastic circular rod dynamical model. Int J Mod Phy b 2021;35:2150168.
[8] Ilhan OA, Bulut H, Sulaiman TA, Baskonus HM. On the new wave behavior of the Magneto-Electro-Elastic (MEE) circular rod longitudinal wave equation. Int J Optim Control: Theor Appl 2020;10:1–8.
[9] Rizvi STR, Seadawy AR, Ahmed S, Ashraf F. Novel rational solitons and generalized breathers for (1+1)-dimensional longitudinal wave equation. Int J Mod Phy b 2023;23:50269.
[10] Younis M, Ali S. Bright, dark, and singular solitons in magneto-electro-elastic circular rod. Waves Random Complex Media 2015;25(4):549–55.
[11] Kumar A, Kumar S, Bohra N. Exploring soliton solutions and interesting wave-form patterns of the (1 + 1)-dimensional longitudinal wave equation in a magnetic-electro-elastic circular rod. Opt Quant Electron 2024;56:1029.
[12] Chakraborty A, Gopalakrishnan S. Various numerical techniques for analysis of longitudinal wave propagation in inhomogeneous one-dimensional waveguides. Acta Mech 2003;162:1–27.
[13] Noufe HA, Reham GA, Seadawy AR. Stability analysis and soliton solutions for the longitudinal wave equation in magneto electro-elastic circular rod. Results Phys 2021;26:104329.
[14] Gopalakrishnan S, Raut MS. Longitudinal wave propagation in one-dimensional waveguides with sinusoidally varying depth. J Sound Vib 2019;463:114945.
[15] Miah MM, Ashik Iqbal M, Osman MS. A study on stochastic longitudinal wave equation in a magneto-electro-elastic annular bar to find the analytical solutions *Commun.* Theor Phys 2023;75:085008.
[16] Aisha A, Attia Raghda A, Alzaidi Jameel AM, Dianchen FL, Khater MA. Analytical and semi-analytical wave solutions for longitudinal wave equation via modified auxiliary equation method and Adomian decomposition method. Therm Sci 2019; 23(6):1943–57.
[17] Ozdemir N, Secer A, Bayram M. Extraction of soliton waves from the longitudinal wave equation with local M-truncated derivatives. Opt Quant Electron 2023;55: 313.
[18] Bulut H, Sulaiman TA, Baskonus HM. On the solitary wave solutions to the longitudinal wave equation in MEE circular rod. Opt Quant Electron 2018;50:87.
[19] Wang K, Zhou J, Xu D, Ouyang H. Lower band gaps of longitudinal wave in a one-dimensional periodic rod by exploiting geometrical nonlinearity. Mech Syst Signal Process 2019;124:664–78.
[20] Darwish A, Seadawy AR, Hamdy MA, Elbably AL, Shehab MF, Arnous AH. Study on soliton solutions of the longitudinal wave equation and magneto-electro-elastic circular rod dynamical model. Int J Mod Phys b 2021;35:2150168.
[21] Ghanbari B, Kumar D, Singh J. Exact solutions of local fractional longitudinal wave equation in a magneto-electro-elastic circular rod in fractal media. Indian J Phys 2022;96:787–94.

[22] Younas U, Sulaiman TA, Ren J. On the optical soliton structures in the magneto electro-elastic circular rod modeled by nonlinear dynamical longitudinal wave equation. Opt Quant Electron 2022;54:688.
[23] Seadawy AR, Rehman SU, Younis M, Rizvi STR, AlthobaitI S, Makhlouf MM. Modulation instability analysis and longitudinal wave propagation in an elastic cylindrical rod modelled with Pochhammer-Chree equation. Phys Scr 2021;96:045202.
[24] Yang XJ. General fractional derivatives: theory, methods and applications. CRC Press; 2019.
[25] Wu GC. Variational iteration method for solving the time-fractional diffusion equations in porous medium. Chin Phys B 2012;21(12):120504.
[26] Wu GC. A fractional variational iteration method for solving fractional nonlinear differential equations. Comput Math Appl 2011;61(8):2186–90.
[27] Gu CY, Wu GC, Shiri B. An inverse problem approach to determine possible memory length of fractional differential equations. Fract Calc Appl Anal 2021;24 (6):1919–36.
[28] Sun H, Chang A, Zhang Y, Chen W. A review on variable-order fractional differential equations: mathematical foundations, physical models, numerical methods and applications. Fract Calc Appl Anal 2019;22(1):27–59.
[29] Khatun MM, Akbar MA. New optical soliton solutions to the space-time fractional perturbed Chen-Lee-Liu equation. Results Phys 2023;46:106306.
[30] Akbar MA, Abdullah FA, Khatun MM. Diverse geometric shape solutions of the time-fractional nonlinear model used in communication engineering. Alexandria Eng J 2023;68:281–90.
[31] Khan H, Li Y, Khan A. Existence of solution for a fractional-order Lotka-Volterra reaction-diffusion model with Mittag-Leffler kernel. Math Methods Appl Sci 2019;42(9):3377–87.
[32] Tajadodi H, Khan ZA, Irshad AUR, Gómez-Aguilar JF, Khan A, Khan H. Exact solutions of conformable fractional differential equations. Results Phys 2021;22:103916.
[33] J. Vanterler da C. Sousa, E. Capelas de Oliveira,. A New Truncated M-Fractional Derivative Type Unifying Some Fractional Derivative Types with Classical Properties. Int J Anal Appl 2018;16(1):83–96.
[34] Roshid MM, Rahman MM, Roshid HO, Bashar MH. A variety of soliton solutions of time M-fractional: Non-linear models via a unified technique. PLoS One 2024;19:e0300321.
[35] Roshid MM, Rahman MM, Roshid HO, Bashar MH, Hossain MM, Mannaf MA. Dynamical simulation of wave solutions for the M-fractional Lonngren-wave equation using two distinct methods. Alexandria. Eng J 2023;81:460–8.
[36] Jawad AJM, Petković MD, Biswas A. Modified simple equation method for nonlinear evolution equations. Appl Math Comput 2010;217:869–77.
[37] Roshid MM, Rahman MM, Roshid HO. Exact and Explicit Traveling Wave Solutions to Two Nonlinear Evolution Equations Which Describe Incompressible Viscoelastic Kelvin-Voigt Fluid Heliyon 2018;4(8):e00756.
[38] Roshid MM, Bairagi T, Rahman MM. Lump, interaction of lump and kink and solitonic solution of nonlinear evolution equation which describe incompressible viscoelastic Kelvin-Voigt fluid. Partial Differential Equations in Applied Mathematics 2022;5:100354.
[39] Zayed EME, Arnous AH. Exact Solutions of the Nonlinear ZK-MEW and the Potential YTSF Equations Using the Modified Simple Equation Method. AIP Conf Proc 2012;1479:2044–8.
[40] Wazwaz AM. Multiple-soliton solutions for the KP equation by Hirota's bilinear method and by the tanh–coth method. Appl Math Comput 2007;190(1):633–40.
[41] Rani A, Ul-Hassan QM, Ayub K, Ahmad J, Zulfiqar A. Soliton solutions of nonlinear evolution equations by basic (G'/G)-expansion method. Math Model Eng Probl 2020;7(2):242–50.
[42] Roshid MM, Rahman MM. Bifurcation analysis, modulation instability and optical soliton solutions and their wave propagation insights to the variable coefficient nonlinear Schrdinger equation with Kerr law nonlinearity. Nonlinear Dy 2024, 2024,:1–23.
[43] Roshid MM, Rahman MM, Roshid HO, Bashar MH. A variety of soliton solutions of time M-fractional: Non-linear models via a unified technique. PLoS One 2024;19 (4):e0300321.
[44] Osman MS, Korkmaz A, Rezazadeh H. The unified method for conformable time fractional Schrö dinger equation with perturbation terms. Chin J Phys 2018;56(5):2500–6.
[45] M.M. Roshid M.M. Alam O.A., İlhan, M.A. Rahim, M.M. Tuhin, M.M. Rahman, Modulation instability and comparative observation of the effect of fractional parameters on new optical soliton solutions of the paraxial wave model Opt. Quantum Electron. 56 6 (2024) 1010.
[46] Xing L, Ma WX, Yu J, Khalique CM. Solitary waves with the Madelung fluid description: A generalized derivative nonlinear Schrödinger equation. Commun Nonlinear Sci Numer Simul 2016;31(1–3):40–6.
[47] Roshid MM, Hossain MM, Hasan MS, Munshi MJH, Sajib AH. Dynamical structure of truncated M− fractional Klein-Gordon model via two integral schemes. Results Phys 2023;46:106272.
[48] Tripathy A, Sahoo S, Rezazadeh H, Izgi ZP, Osman MS. Dynamics of damped and undamped wave natures in ferromagnetic materials. Optik 2023;281:170817.
[49] Roshid MM, Abdeljabbar A, Begum M, Basher H. Abundant dynamical solitary waves through Kelvin-Voigt fluid via the truncated M-fractional Oskolkov model. Results Phys 2023;55:107128.
[50] Gu M, Peng C, Li Z. Traveling wave solution of (3+1)-dimensional negative-order KdV-Calogero-Bogoyavlenskii-Schiff equation. AIMS Math 2024;9(3):6699–708.
[51] Han T, Zhang K, Jiang Y, Rezazadeh H. Chaotic Pattern and Solitary Solutions for the (21)-Dimensional Beta-Fractional Double-Chain DNA System. Fractal Fract 2024;8(7):415.
[52] Mamunur Roshid M, Abdeljabbar A, Aldurayhim A, Rahman M, Roshid H-O, Alshammari F. Dynamical interaction of solitary, periodic, rogue type wave solutions and multi-soliton solutions of the nonlinear models. Heliyon 2022;8(12):e11996. https://doi.org/10.1016/j.heliyon.2022.e11996.